Chemical Science

ROYAL SOCIETY OF CHEMISTRY

EDGE ARTICLE

View Article Online
View Journal | View Issue

Cite this: *Chem. Sci.*, 2025, **16**, 13816

All publication charges for this article have been paid for by the Royal Society of Chemistry

Received 18th April 2025
Accepted 23rd June 2025

DOI: 10.1039/d5sc02854j

rsc.li/chemical-science

Photoredox-catalyzed regioselective allene alkoxycarbonylations for the synthesis of α-allyl-γ-lactones†

Elijah T. Marris,[a] Ashley L. Palecek,[a] Federico Barbieri,[ab] Derek B. Hu,[a] Ken S. Lee[a] and Jennifer M. Schomaker *[a]

A dual photoredox/hydrogen atom transfer (HAT) strategy for the radical alkoxycarbonylation of allenes is described. Alkoxycarbonyl radicals, generated by photoredox-catalyzed decarboxylation of alkyl oxalic acids, add to the proximal carbon of allene precursors with high regioselectivity to furnish α-allyl-γ-lactone products in up to 92% yield. The intermediate vinyl radicals can be trapped by a hydrogen atom or by a heteroatom using selenium and iodine transfer reagents. The alkene and vinyl moieties are readily post-functionalized to furnish more complex molecular scaffolds, highlighting the synthetic utility offered using the combination of allenes and oxalic acids as compared to their alkene and oxalate salt counterparts.

Introduction

Lactones are produced by plants, marine sponges, bacteria, fungi, and a variety of other organisms;[1] reports estimate that the γ-lactone motif is found in nearly 10% of all natural products.[2] A subset of these compounds, α-allyl-γ-lactones, exhibit diverse biological profiles that include antifungal, antitumor, antiviral, anti-inflammatory, and antibiotic properties (Fig. 1A).[3–6] However, the lack of conjugation between the alkene and the lactone carbonyl has made direct synthetic approaches to this scaffold challenging to achieve. General methods for the syntheses of γ-lactones primarily focus on polar or oxidative methods to target the formation of C–O bonds. Commonly used strategies include Baeyer–Villiger oxidation, intramolecular esterifications of hydroxy acids, and iodolactonization reactions (Fig. 1B).[7] In contrast, alternative methods able to construct the C–C(O) bond of lactones have been historically underexplored in the literature. Despite scattered examples reporting the formation of C–C(O) bonds using selenocarbonates, Barton esters, and *S*-alkoxycarbonyl xanthates as acyl radical precursors, the limited scope, poor yields, harsh conditions, toxic reagents, and the need to cleave undesired residual functional groups have hindered their broad synthetic utility.[8–12] Thus, a strategy capable of forming the C–C(O) bond of an ester under mild reaction conditions with good functional group tolerance, coupled with the ability to capture an intermediate radical species with diverse trapping agents, is an appealing approach to the synthesis of γ-lactones (Fig. 1B).

Given the recent emergence of myriad modern synthetic methods that provide facile access to allenes,[13–16] the lack of selective, photoredox-catalyzed additions of radicals to these intriguing building blocks is surprising. Allenes offer advantages over typical alkenes; first, they tend to display higher reactivity compared to the corresponding alkenes, due to increased strain in the ground state imparted by the cumulated double bonds.[17] Second, the two cumulated allene π-bonds span three contiguous unsaturated carbons, offering three potential sites for functionalization, as opposed to two sites for an alkene. Third, addition of a radical to an allene acceptor can furnish a high energy vinyl radical intermediate that may be captured with diverse trapping agents to yield residual alkenes or vinyl moieties as handles for further post-functionalization. Finally, the axial chirality inherent in many allenes offers the potential to achieve precise stereocontrol *via* axial-to-point chirality transfer without the need for a chiral catalyst.[17]

Our group previously reported the addition of amidyl radicals to allenes (Fig. 2A) to furnish the corresponding γ-lactams and carbamates.[18] While attack at the β (central) allene carbon *via* a 6-*exo*/*endo*-dig cyclization might be expected, as it yields a thermodynamically more stable allylic radical, the orthogonality of the allene π system necessitates a 90° orbital rotation after the addition to bring the radical into conjugation with the remaining π bond (Fig. 2B). The additional energy required for such a rotation often favors the kinetic formation of a vinyl radical.[18–21] Due to these additional stereoelectronic considerations, selectivity rules in radical-based allene cyclizations have not been extensively studied or well defined. While 6-*exo*/*endo*-

[a]*Department of Chemistry, University of Wisconsin–Madison, 1101 University Avenue, Madison, WI 53706, USA. E-mail: schomakerj@chem.wisc.edu*

[b]*Department of Chemistry, University of Pavia, Via Torquato Taramelli, 12, 27100 Pavia PV, Italy*

† Electronic supplementary information (ESI) available. See DOI: https://doi.org/10.1039/d5sc02854j

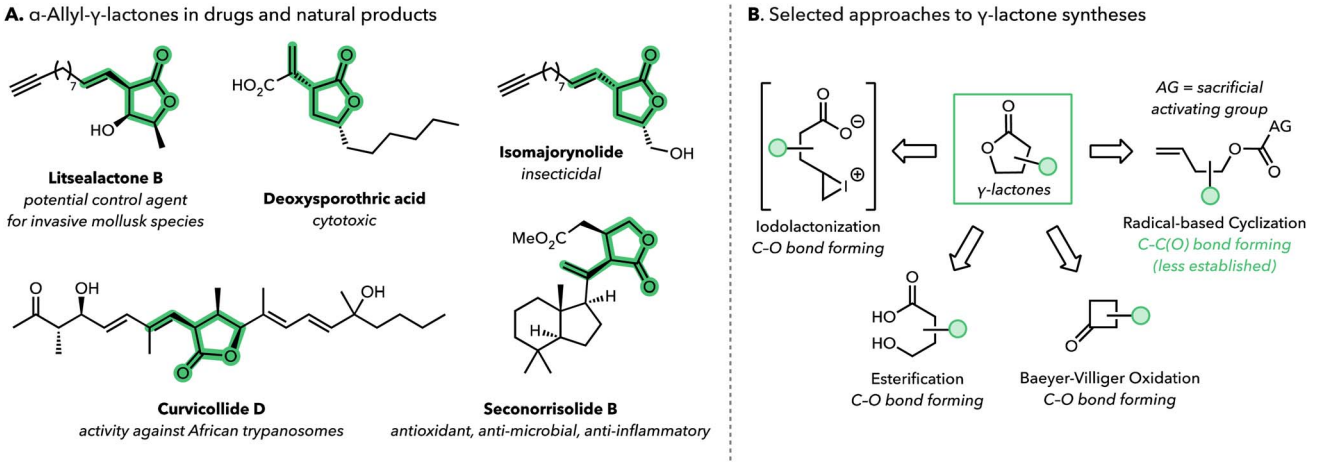

Fig. 1 (A) Bioactive α-allyl-γ-lactones. (B) Approaches to the syntheses of γ-lactones.

dig cyclizations to an allylic radical are allowed according to Baldwin's rules, the reaction of *N*-centered radicals only occurred at the α (proximal) carbon in a 5-*exo*-trig fashion, despite the formation of a high energy vinyl radical intermediate.[22] We originally theorized that the observed regioselectivity was due to the aforementioned high energy barrier of rotation required to bring the radical resulting from attack at the β carbon of the allene into conjugation with the remaining alkene. However, recent computations by our group have shown that the α carbon of these pendant allenes is more electron-rich than the β carbon; thus, selective 5-*exo*-trig cyclizations may also be favorable due to a polarity match between the electrophilic amidyl radical and the α allene carbon (see the ESI† for details).[23]

The goal of this work was to expand the diversity of radicals that add to allenes in a predictable and selective manner. Specifically, we were curious whether a weakly nucleophilic alkoxycarbonyl radical, which represents a polarity mismatch with the electron-rich proximal α-carbon of an allene, would result in a different regioselectivity in the radical addition step, or whether kinetics would dictate the formation of valuable α-allyl-γ-lactone products (Fig. 2C).[23] Herein, we report mild and

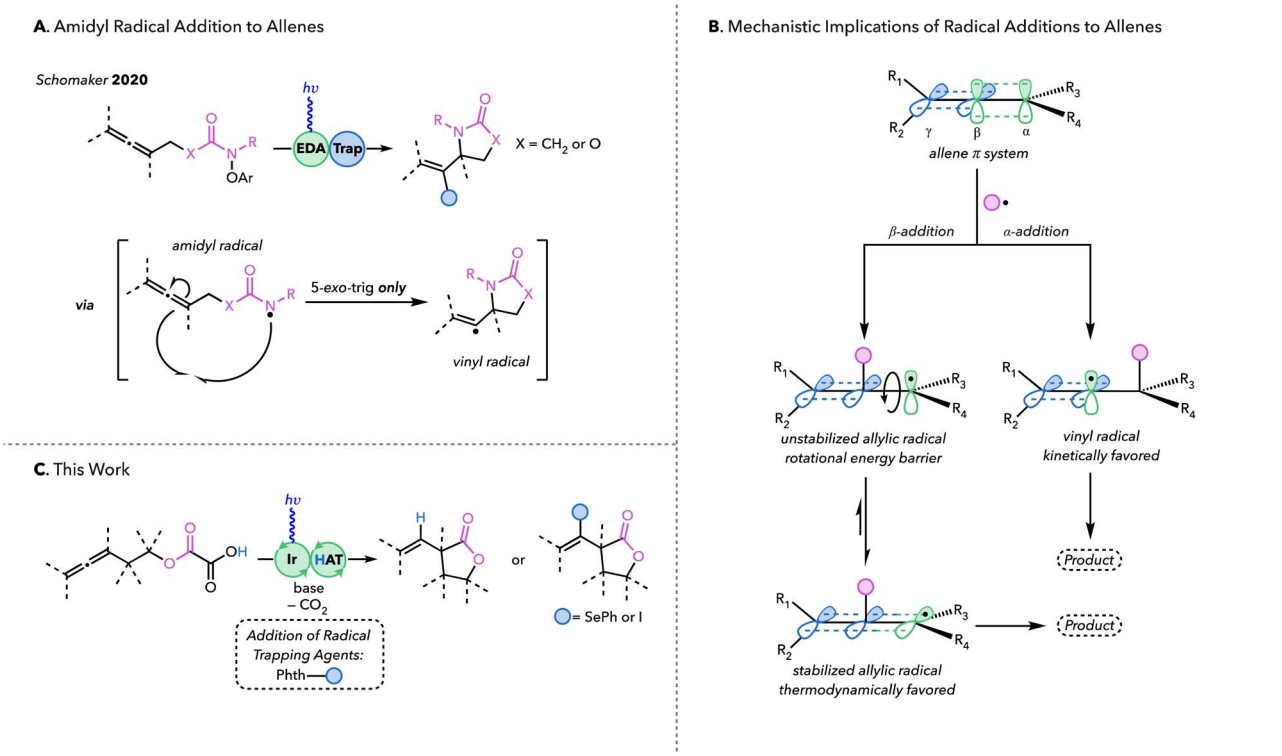

Fig. 2 Proposed work and mechanistic implications of radical additions to allenes.

convenient conditions for regioselective allene alkoxycarbonylations using dual photoredox/hydrogen atom transfer (HAT) catalysis; to the best of our knowledge, this constitutes the first example of any acyl-type radical addition to allenes. Highlights of the method include the use of convenient oxalic acids instead of typical cesium oxalate salts, good allene scope, high regioselectivity for formation of α-allyl-γ-lactones, mild reaction conditions, and the ability to intercept the high-energy vinyl radical intermediates with diverse trapping agents to install a terminal C–H or C–X (where X = Se or I) bond on the remaining alkenes, which can be engaged in versatile post-functionalizations.

Results and discussion

Research strategy and approach

Early photoredox-catalyzed methods to generate alkoxycarbonyl radicals used *N*-phthalimidoyl oxalates (Fig. 3).[24] These species are reduced by an excited photocatalyst, resulting in the loss of CO_2 and phthalimide to furnish the radical. The need for a stoichiometric sacrificial reductant (*e.g.*, a Hantzsch ester), coupled with the instability of *N*-phthalimidoyl oxalates towards aqueous workup and flash chromatography, has prompted the alternative use of oxalate salts (typically cesium salts) as alkoxycarbonyl radical precursors.[24,25] Oxidation of the oxalate salt by an excited photocatalyst triggers rapid decarboxylation to deliver the alkoxycarbonyl radical. In contrast, alkyl oxalic acids have rarely been used as radical precursors due to their instability and tendency to disproportionate into dialkyl oxalates and oxalic acid ($[COOH]_2$) even when stored at low temperatures.[25] Nevertheless, we found that diluting alkyl oxalic acids with ethereal solvents at −20 °C permits their long-term storage and use as robust and convenient radical precursors. We observed no significant decrease in purity after 6 months of storage. Alkyl oxalic acids offer three distinct advantages over oxalate salts. First, most alkyl oxalic acids are easily synthesized in one step from the reaction of the corresponding alcohol with oxalyl chloride with no need for purification. In contrast, the synthesis of oxalate salts is typically a multi-step process involving the reaction of the alcohol with an alkyl chlorooxoacetate, followed by purification and subsequent saponification. Second, oxalate salts often display poor solubility in common organic solvents.[25–27] Lastly, the proton of our oxalic acid precursors may be used as an eventual source of H˙ by incorporation by a base into the HAT cycle.

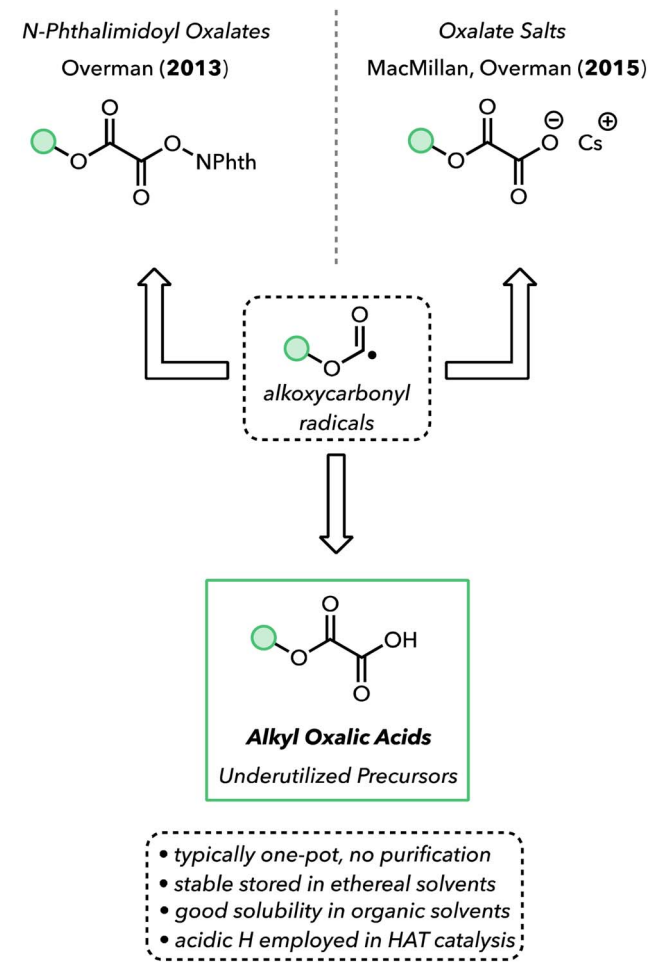

Fig. 3 Precursors in photoredox-catalyzed generation of alkoxycarbonyl radicals.

We drew inspiration from Overman's nickel/photoredox spirolactonization chemistry using alkenes and cesium oxalate salts, with the proposed mechanism in Scheme 1 guiding our initial optimizations of allene alkoxycarbonylation employing alkyl oxalic acids as radical precursors.[28] First, deprotonation (PT) of the homoallenic oxalic acid generates an oxidizable alkyl oxalate and a conjugate acid. Concurrently, excitation of an iridium photocatalyst results in a highly oxidizing Ir^{III}* species. Single electron transfer (SET) from the alkyl oxalate to the excited photocatalyst, followed by loss of CO_2, was hypothesized to give a reactive alkoxycarbonyl radical and a reduced Ir^{II} photocatalyst. Addition of the C-centered radical to the α carbon of the allene *via* a 5-*exo*-trig cyclization yields a vinyl radical, which abstracts H˙ from a thiol HAT catalyst to furnish an α-allyl-γ-lactone and a thiyl radical. The S-centered radical is turned over by the reduced photocatalyst *via* single electron reduction to give a thiolate and regenerate Ir^{III}. Finally, the thiolate deprotonates the aforementioned conjugate acid to complete the HAT cycle. Notably, theoretical use of an alkene instead of an allene would result in a relatively long-lived alkyl radical following addition, which would be capable of either reductive radical polar crossover (without the need for an HAT catalyst) to turn over the photoredox catalytic cycle or interception by a transition metal catalyst. However, reductive radical polar crossover of the shorter-lived vinyl radical to a vinyl anion is thermodynamically challenging in the absence of harsh reductants. Thus, we hypothesized that a synergistic HAT catalysis cycle would be required in our chemistry to intercept the reactive vinyl radical and to turn over the photocatalyst.

Before choosing reaction conditions for the proposed system in Scheme 1, we carefully considered the redox potentials of a deprotonated alkyl oxalate, the photocatalyst, and the HAT catalyst. $[Ir(dFCF_3ppy)_2\text{-}(5,5'\text{-}dCF_3bpy)]PF_6$ (**PC1**) ($E_{1/2}[*Ir^{III}/Ir^{II}]$

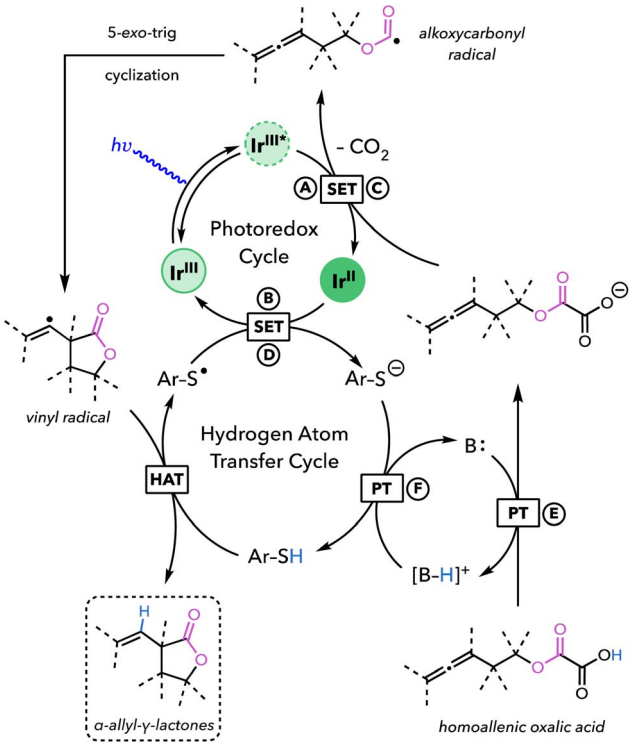

Scheme 1 Proposed reaction mechanism.

$= +1.68$ V *vs.* SCE and $E_{1/2}[Ir^{III}/Ir^{II}] = -0.69$ V *vs.* SCE) (**A** and **B**) was expected to be a suitable photocatalyst, as it is capable of oxidizing a deprotonated alkyl oxalate ($E_{1/2} = +1.28$ V *vs.* SCE for *t*-BuOC(O)CO_2Cs) (**C**) and reducing an aryl thiyl radical intermediate ($E_{1/2}$ [PhS$^{\bullet}$/PhS^{-}] = +0.16 V *vs.* SCE) (**D**).[28–30] The pK_a values of the alkyl oxalic acid, the HAT catalyst, and the base were also determined to ensure favorable acid/base equilibria. While pK_a values are dependent on the solvent, a base whose conjugate acid has an approximate pK_a value between 2 and 6 was an ideal starting point, as deprotonation of the alkyl oxalic acid (pK_{a_1} of oxalic acid ≈ 1.27) (**E**) and protonation of the thiolate (pK_a of thiophenol ≈ 6.62) (**F**) would be favorable.[31,32] Thus, initial screening efforts employed pyridine as the base, as pyridinium has a pK_a value of 5.23.[31] We also selected 2,4,6-triisopropyl-thiophenol (TRIP thiol), due to its high compatibility as an HAT catalyst when used in tandem with **PC1** and other photocatalysts.[33]

Reaction optimization

Treatment of 2-(hexa-3,4-dien-1-yloxy)-2-oxoacetic acid (**1**) as a model allene with 2 mol% of **PC1**, 20 mol% of TRIP thiol, and 1.25 equivalents of pyridine provided the resulting α-allyl-γ-lactone **3** in 20% NMR yield following irradiation with blue LEDs in 1,4-dioxane at room temperature (Table 1, entry 1). Several bases whose conjugate acids have similar pK_a values to pyridinium were explored next. The organic bases 2,6-lutidine and *N*-methylimidazole (NMI) increased the reaction yields to 33% and 36%, respectively (entries 2, 3). The inorganic bases Cs_2CO_3 and Na_2HPO_4 resulted in undesired polymerization or decomposition (entries 4, 5). Switching the standard blue LEDs for a 456 nm Kessil lamp increased the yield of **3** to 46% (entry 6), likely due to improvement in the light penetration and better absorption by the photocatalyst, as well as a slight increase in temperature. A screen of solvents (see S23 in the ESI† for details) and solvent mixtures was also conducted, but no improvement in reaction yield or conversion was observed.

Next, the identity of the HAT catalyst was optimized by testing various aromatic, aliphatic, and silylated thiols. While other thiol hydrogen atom donors were moderately successful, TRIP thiol was the optimal HAT catalyst, as the presence of different substituents on the aromatic ring of thiophenol derivatives have only minor effects on the S–H bond strength. However, changing these substituents can result in large variations in the pK_a and redox potentials of the thiophenols.[30,34] Since TRIP thiol is already known to synergize well with **PC1** and had been employed throughout our base optimization study, no further optimization was conducted. We expected that any significant changes to redox potentials or pK_a of the thiol HAT catalyst were likely to have a detrimental effect on the reaction outcome.

Other photocatalysts were explored in addition to **PC1**, where the yields showed a moderate correlation with the excited state potentials of the iridium photocatalyst. The less oxidizing [Ir(dF(CF_3)ppy)$_2$(dtbpy)]PF_6 (**PC2**) and [Ir(dF(Me)ppy)$_2$(dtbpy)]PF_6 (**PC3**) gave poor yields (entries 7 and 8), whereas the more oxidizing [Ir(dCF_3(CF_3)ppy)$_2$-(5,5′-dCF_3bpy)]PF_6 (**PC4**) ($E_{1/2}$-[*Ir_{III}/Ir^{II}] = +1.81 V *vs.* SCE) (entry 9) slightly increased the yield to 48%.[33] Ruthenium-based and organic photocatalysts (*e.g.* 4CzIPN) were not successful. A 3 mol% loading of **PC4** improved the yield to 56% (entry 10), while a decrease to 1 mol% or an increase >4 mol% gave diminished yields, likely due to self-quenching in the latter case (entries 11 and 12).

To further enhance the yields, the counteranion of the photocatalyst **PC4** was optimized. Knowles and coworkers demonstrated that the coordinating ability of counteranions to iridium catalysts can impact their excited-state redox potentials, excited-state lifetimes, and the kinetics of single-electron transfer events. Specifically, changing from the $^{-}PF_6$ counteranion of **PC4** to $^{-}$OTf extended the photocatalyst's excited state lifetime by 263 ns and increased the rate of initial aniline oxidation to the aminium radical cation by 0.4×10^{-7} M^{-1} s^{-1}.[33] Accordingly, we prepared two derivatives of **PC4** by replacing the $^{-}PF_6$ counteranion with either $^{-}BAr^{F}{}_4$ (**PC4**$_{BARF}$) or $^{-}$OTf (**PC4**$_{OTf}$). Unsurprisingly, the weakly coordinating ion-pair **PC4**$_{BARF}$ decreased the yield of **1a** 44%, whereas the strongly coordinating ion-pair **PC4**$_{OTf}$ increased the yield of **1a** to 62% (entries 13, 14).

Given the inherent high energy of vinyl radical species and the polarity mismatch between the alkoxycarbonyl radical and the proximal allene carbon, the rate of cyclization was expected to be relatively slow.[23,35] Gratifyingly, we found that gem-dimethyl substitution on the aliphatic chain of **2** improved the yield of **2a** to 80% (entry 15), presumably due to the Thorpe-Ingold effect. Finally, decreasing the reaction concentration to 0.075 M furnished α-allyl-γ-lactone **2a** in 84% isolated yield (entry 16). In a series of control reactions, omitting the

Table 1 Reaction optimization[a]

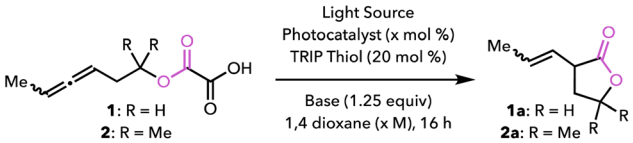

Entry	Starting material	Base	Light source	Photocatalyst	Conc.	Lactone yield (%)
1	**1**	Pyridine	Blue LEDs	**PC1** (2 mol%)	0.125 M	20
2	**1**	2,6-lutidine	Blue LEDs	**PC1** (2 mol%)	0.125 M	33
3	**1**	NMI	Blue LEDs	**PC1** (2 mol%)	0.125 M	36
4	**1**	Cs_2CO_3	Blue LEDs	**PC1** (2 mol%)	0.125 M	0
5	**1**	Na_2HPO_4	Blue LEDs	**PC1** (2 mol%)	0.125 M	0
6	**1**	NMI	456 nm Kessil	**PC1** (2 mol%)	0.125 M	46
7	**1**	NMI	456 nm Kessil	**PC2** (2 mol%)	0.125 M	8
8	**1**	NMI	456 nm Kessil	**PC3** (2 mol%)	0.125 M	23
9	**1**	NMI	456 nm Kessil	**PC4** (2 mol%)	0.125 M	48
10	**1**	NMI	456 nm Kessil	**PC4** (3 mol%)	0.125 M	56
11	**1**	NMI	456 nm Kessil	**PC4** (1 mol%)	0.125 M	8
12	**1**	NMI	456 nm Kessil	**PC4** (4 mol%)	0.125 M	54
13	**1**	NMI	456 nm Kessil	$\mathbf{PC4}_{BARF}$ (3 mol%)	0.125 M	44
14	**1**	NMI	456 nm Kessil	$\mathbf{PC4}_{OTf}$ (3 mol%)	0.125 M	62
15	**2**	NMI	456 nm Kessil	$\mathbf{PC4}_{OTf}$ (3 mol%)	0.125 M	80
16	**2**	NMI	456 nm Kessil	$\mathbf{PC4}_{OTf}$ (3 mol%)	0.075 M	84[b]
17	**2**	NMI	456 nm Kessil	None	0.075 M	0
18	**2**	NMI	None	$\mathbf{PC4}_{OTf}$ (3 mol%)	0.075 M	0
19	**2**	None	456 nm Kessil	$\mathbf{PC4}_{OTf}$ (3 mol%)	0.075 M	Trace
20[c]	**2**	NMI	456 nm Kessil	$\mathbf{PC4}_{OTf}$ (3 mol%)	0.075 M	15

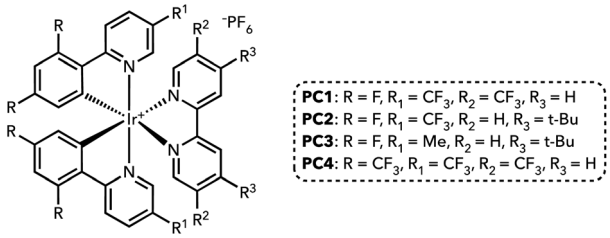

[a] Unless otherwise noted, yields were obtained using ^{1}H NMR with mesitylene as the internal standard. [b] Isolated yield. [c] Omission of TRIP Thiol.

photocatalyst, base, or light all gave either no or trace amounts of **2a**. Poor yields from these control experiments are consistent with our current mechanistic hypothesis (entries 17–19). The absence of TRIP thiol gave 15% yield of **2a** (entry 20), suggesting that minor amounts of the vinyl radical intermediate may be quenched by the solvent.

Scope and other results

With the optimized hydro-alkoxycarbonylation conditions in hand, the allene scope was explored. The resulting α-allyl-γ-lactone products are depicted in Table 2. The model substrate **2** furnished **2a** in 84% isolated yield and a 3.9 : 1 *E* : *Z* ratio on a 0.25 mmol scale. The size of the alkyl or aryl substituent at the distal allene carbon could be varied broadly to provide the desired lactones in good-to-excellent yields (**3a**, **4a**, **5a**, and **6a**). Interestingly, there was no clear correlation between the size of the distal allene substituent and the *E* : *Z* ratio of the resultant alkenes. Trisubstituted allenes were also well tolerated, giving **7a**, **8a**, and **9a** in 71%, 75%, and 71% yield, respectively. Monosubstituted allenes also cyclized smoothly, resulting in α-allyl-γ-lactones **10a**, **11a**, **12a**, **13a**, and **14a** in up to a 92% isolated yield. Altering the substituents directly adjacent to the oxalic acid had no detrimental impact on product formation, as evidenced by good yields of gem-diethyl and gem-dibenzyl lactones **11a** and **15a**, along with the spirolactones **12a**, **13a** and **14a**. Substitution at the other position of the tether resulted in diminished yields (**16a**, **17a**, and **18a**), often with recovered allene. Steric hindrance adjacent to the α carbon of the allene and/or an unfavorable geometry in the cyclization transition state may be responsible for these results. A large-scale reaction (2.50 mmol, 10× standard conditions) provided **10a** in a 64% isolated yield with full conversion of **10**, thereby highlighting the scalability of this method.

Table 2 Scope of the regioselective alkoxycarbonylation of allenes[a]

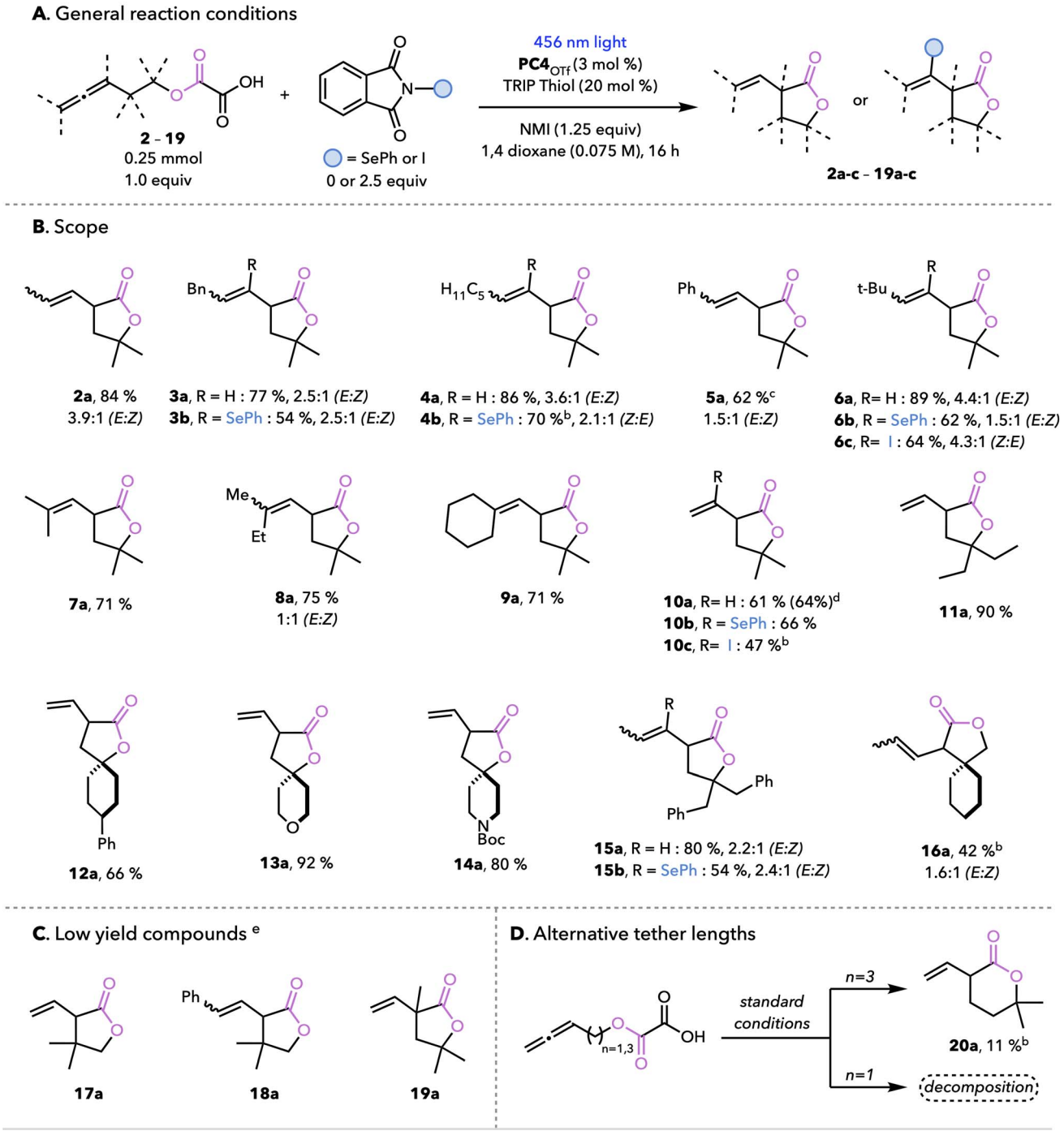

[a] Unless otherwise noted, isolated yields are provided. [b] Yields obtained using ^{1}H NMR with mesitylene as the internal standard. [c] Approximately 9% δ-lactone formation. [d] Run at a 2.50 mmol scale (10× scale-up from standard conditions). [e] Less than 20% ^{1}H NMR yield.

After having expanded the scope of allene hydro-alkoxycarbonylations from homoallenic alkyl oxalic acids, precursors with different tether lengths between the allene and the oxalic acid were explored (Table 2D). A three-carbon tether in **20** formed the δ-lactone **20a** in an 11% NMR yield. Employing an allene starting material with a one carbon tether could provide access to valuable β-lactones *via* addition to the α carbon of the allene, γ-lactones through addition to the β carbon, or δ-lactones by addition to the γ carbon. Unfortunately, all attempts resulted in decomposition.

We next investigated the possibility of forming value-added alkenes by intercepting the vinyl radical with other atom transfer reagents in addition to TRIP thiol. An extensive screening of diverse radical traps (see S26 in the ESI† for details) revealed that *N*-(phenylseleno)phthalimide and *N*-iodophthalimide were competent additives for capping the vinyl radical with either selenium or iodine, respectively. Complete removal of TRIP thiol in the presence of either *N*-(phenylseleno) phthalimide or *N*-iodophthalimide still gave the desired product, albeit in diminished yields. These control experiments imply two possible pathways for forming the seleno- or iodo-trapped products. In both cases, the vinyl radical abstracts either the selenium or iodine from the phthalimide to form the desired product and an *N*-centered phthalimide radical. In the absence of an HAT catalyst, the nitrogen radical may undergo reductive radical polar crossover with the Ir^{II} catalyst to turn over the photoredox catalyst and form the phthalimide anion, which can then deprotonate the conjugate acid of NMI. In the presence of an HAT catalyst, the phthalimide radical may alternatively abstract H˙ directly from TRIP thiol, enabling the thiyl radical to turn over the iridium catalyst as shown in Scheme 1. *N*-(Phenylseleno)phthalimide and *N*-iodophthalimide trapping agents were tested with various allene precursors to generate the vinyl seleno- or iodo- products **3b**, **4b**, **6b**, **6c**, **10b**, **10c**, and **15b** in yields ranging from 47% to 70% (Table 2, *vide supra*).

Mechanistic studies

To test the validity of our proposed mechanism (Scheme 1, *vide supra*), a TEMPO trapping experiment was performed; reactivity was shut down and the expected vinyl-TEMPO adduct (Fig. 4A) was formed. This result further supports the radical-based nature of our mechanism. Next, a Stern–Volmer quenching study was conducted (Fig. 4B).[36] Unsurprisingly, these data indicate that the excited photocatalyst is most efficiently quenched by a combination of oxalic acid and NMI, whereas protonated oxalic acid leads to poor quenching. While these results support that the excited $\mathbf{PC4}_{OTf}$ indeed oxidizes the oxalic acid substrate in the presence of NMI, a concerted proton coupled electron transfer (PCET) mechanism (over stepwise deprotonation, followed by oxidation) cannot be entirely ruled out.

The presence of axial chirality in many allenes offers the potential to transfer this chirality to point chirality at the α position of the α-allyl-γ-lactone product. Chirality transfer was expected to be straightforward, given that cyclization should form the vinyl radical in a stereoretentive manner, as opposed to ablation of stereochemistry through formation of an allylic radical. However, subjecting enantioenriched **15** to the general reaction conditions furnished only racemic **15a**. While chirality transfer was ultimately unsuccessful, other strategies to achieve stereospecific photoredox-catalyzed allene functionalization are under active investigation in our laboratory. We hypothesized that once the vinyl radical is generated, the α C–H of the lactone becomes even more acidic.[37] Rapid deprotonation forms a radical anion, which leads to racemization. This radical anion may be an example of a "redox upconverted species," as described by Opatz and coworkers.[37] Upconversion *via* deprotonation converts radicals to potent reductants, which act as effective SET-propagating donors to increase the efficiency of

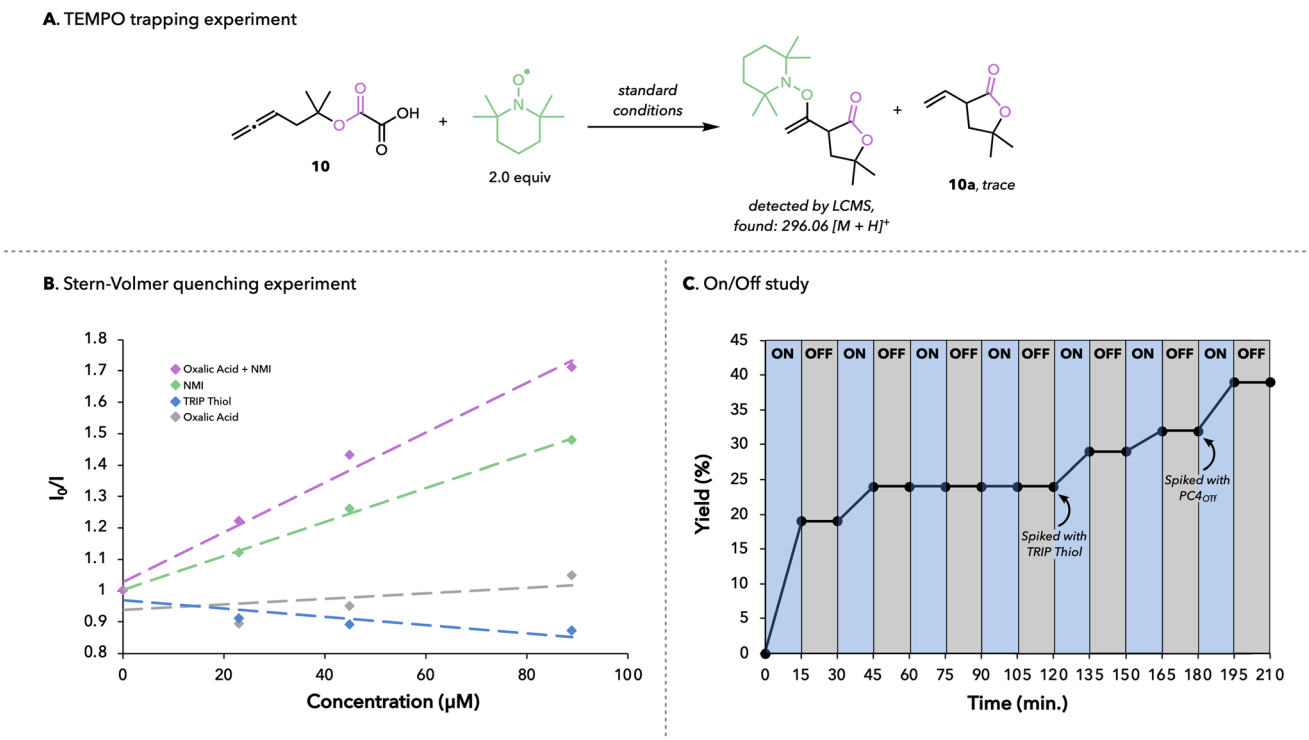

Fig. 4 Mechanistic studies.

photoredox catalysis. To test the possibility of this type of radical chain mechanism, an on/off experiment was conducted with 15-minute intervals (Fig. 4C). Notably, the yield remains stagnant during the off cycles, implying a high likelihood of a closed photoredox cycle as opposed to a radical chain pathway. Given this result, the most probable explanation for racemization is reversible HAT of the α C–H of the lactone with TRIP thiol.[38,39] Interestingly, we noticed that the reaction began to stall after the first few on/off cycles. Upon continuous exposure to light, full consumption of the starting material is typically observed. We propose that stalling occurs due to the buildup of disulfide in the off phases, which effectively removes the active HAT catalyst from the reaction system and compromises catalyst turnover from Ir(II) back to Ir(III). Reactivity is restored after spiking the reaction mixture with either fresh TRIP thiol or fresh $\mathbf{PC4}_{OTf}$.

Post-functionalizations

To showcase the synthetic utility of these unique alkoxycarbonylated products, a variety of post-functionalizations were conducted (Scheme 2). For example, the lactone **10a** could be opened by treatment with MeMgBr to give the 1,4 diol **21** in 96% yield. Isomerization of the alkene in **10a** also proceeded smoothly upon treatment with DBU to furnish the α-methylene-γ-lactone **22** in 76% yield; these scaffolds are of particular interest due to their anti-leukemic properties and prevalence in natural products.[40] Vinyl seleno-**10b** was converted to the allenoate **23** *via* selenoxide elimination in 64% yield.[41] Lastly, the vinyl iodide **6c** was subjected to standard Sonogashira conditions, resulting in cross-coupling to furnish **24** in 43% yield.

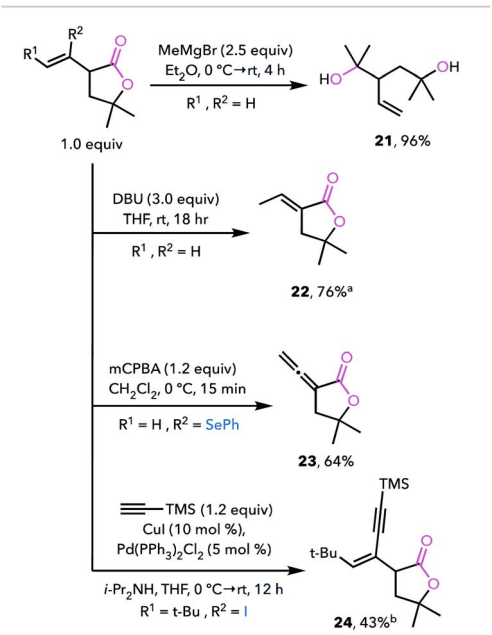

Isolated yields. [a] Only E isomer formation. [b] Decomposition of the E isomer upon purification.

Scheme 2 Product diversifications.

Conclusion

In conclusion, we have developed a dual photoredox/HAT catalysis strategy for the first examples of acyl-type (alkoxycarbonyl) radical addition to allenes. In doing so, we synthesized a variety of α-allyl-γ-lactone products, which would otherwise be challenging to directly access due to the lack of conjugation between the alkene with lactone carbonyl. By employing alkyl oxalic acids instead of oxalate salts, we were also able to streamline starting material synthesis, improve the substrate solubility, and invoke productive hydrogen atom transfer from the precursor to the product. Additionally, the method benefits from the more versatile reactivity of allenes as compared to alkenes, offering high regioselectivity despite a polarity mismatch between the radical and acceptor and the ability to intercept intermediate vinyl radicals with diverse trapping agents. The residual alkene or vinyl seleno- and iodo-moieties can be employed in valuable post-functionalizations for the synthesis of more complex lactone-containing natural products or pharmaceuticals. This work provides useful insights into the application of both allenes and alkyl oxalic acids in the field of photoredox catalysis, opening the door for future reaction design and development. Methods for intermolecular acyl radical additions to allenes, strategies to functionalize all three allene carbons *via* telescoped radical reactions, and the ability to capture allene-derived short-lived vinyl radical intermediates with transition metals are currently under active investigation in our laboratory.

Data availability

The data supporting this article have been included as part of the ESI.† The authors have cited additional references within the ESI.†[42–50]

Author contributions

The manuscript was written through contributions of all authors. All authors have given approval to the final version of the manuscript.

Conflicts of interest

There are no conflicts to declare.

Acknowledgements

J. M. S. is grateful to the NIH (1R35GM152043) and the University of Wisconsin Vilas Associates Award for financial support of this research. The Paul Bender Chemistry Instrumentation Center includes a Thermo Q ExactiveTM Plus from NIH 1S10 OD020022-1; a Bruker Avance-500 as a generous gift from Paul J. and Margaret M. Bender; a Bruker Avance-600 from NIH S10 OK012245; a Bruker Avance-400 from NSF CHE-1048642. Dr Martha M. Vestling at UW-Madison is thanked for mass spectrometry characterization. Dr Heike Hofstetter and the NMR instrumentation staff at UW-Madison are thanked for

advice on structural characterization. Members of the Yoon group at UW-Madison are thanked for useful conversations about photocatalysts and mechanisms. Members of the Boros group at UW–Madison are thanked for access to their fluorometer for quenching studies for constructing Stern–Volmer plots.

References

1 S. K. Sartori, M. A. N. Diaz and G. Diaz-Muñoz, Lactones: Classification, synthesis, biological activities, and industrial applications, *Tetrahedron*, 2021, **84**, 1–39.
2 S. Gil, M. Parra, P. Rodriguez and J. Segura, Recent developments in γ-lactone synthesis, *Mini-Rev. Org. Chem.*, 2009, **6**, 345–358.
3 T. Qiao, Y. Wang, S. Zheng, H. Kang and G. Liang, Total syntheses of norrisolide-type *Spongian* diterpenes Cheloviolene C, Seconorrisolide B and Seconorrisolide C, *Angew. Chem., Int. Ed.*, 2020, **59**, 14111–14114.
4 M. Ortiz-Gonzalez, *et al.*, Curvicollide D isolated from the fungus *Amesia* sp. kills African trypanosomes by inhibiting transcription, *Int. J. Mol. Sci.*, 2022, **23**, 6107.
5 B. M. Fraga, C. E. Díaz, P. Bolaňos, M. Bailén, M. F. Andrés and A. Gonzáles-Coloma, Alkane-, alkene-, alkyne-γ-lactones and ryanodane diterpenes from aeroponically grown *Persea indica* roots, *Phytochemicals*, 2020, **176**, 112398.
6 B. S. Min, S. Y. Lee, J. H. Kim, O. K. Kwon, B. Y. Park, R. B. An, J. K. Lee, H. I. Moon, T. J. Kim, Y. H. Kim, H. Joung and H. K. Lee, Lactones from the leaves of *Litsea japonica* and their anti-complement activity, *J. Nat. Prod.*, 2003, **66**, 1388–1390.
7 D. Cavalli and J. Waser, Organic Dye Photocatalyzed synthesis of functionalized lactones and lactams *via* a cyclization–alkynylation cascade, *Org. Lett.*, 2024, **26**, 4235–4239.
8 M. D. Bachi and E. Bosch, Desilylation of α-Trimethylsilylmethylene-δ-Lactones. A New Route to α-Methylene-δ-Lactones, *Tetrahedron Lett.*, 1988, **29**, 2581–2584.
9 M. D. Bachi and E. Bosch, Synthesis of γ- and δ-Lactones by Free-Radical Annelation of Se-Phenyl Selenocarbonates, *J. Org. Chem.*, 1992, **57**, 4696–4705.
10 H. Togo and M. Yokoyama, One-Pot Preparation of g-Butyrolactone Derivatives from Olefinic Alcohols *Via* Intramolecular Radical Cyclization, *Heterocycles*, 1990, **31**, 437–441.
11 H. Togo, M. Fujii and M. Yokoyama, Conversion of Hydroxyl Groups in Alcohols to Other Functional Groups with N-Hydroxy-2-thiopyridone, and Its Application to Dialkylamines and Thiols, *Bull. Chem. Soc. Jpn.*, 1991, **64**, 57–67.
12 J. E. Forbes, R. N. Saicic and S. Z. Zard, New Radical Reactions of S-Alkoxycarbonyl Xanthates. Total Synthesis of (±)-Cinnamolide and (±)-Methylenolactocin, *Tetrahedron*, 1999, **55**, 3791–3802.
13 J. Singh, B. Saxena and A. Sharma, Visible light promoted synthesis of allenes, *Catal. Sci. Technol.*, 2024, **14**, 5143–5260.
14 S. Li, K. Yuan, G. Zhang and R. Guo, Recent advances in the synthesis of chiral allenes *via* asymmetric 1,4-difunctionalization of 1,3-enynes, *Eur. J. Org. Chem.*, 2024, **27**, e202301316.
15 Y. Li and H. Bao, Radical transformations for allene synthesis, *Chem. Sci.*, 2022, **13**, 8491–8506.
16 R. J. Armstrong, Synthesis of allenes by 1,2-elimination, *Curr. Org. Chem.*, 2019, **23**, 3027–3039.
17 L. Lui, R. M. Ward and J. M. Schomaker, Mechanistic Aspects and Synthetic Applications of Radical Additions to Allenes, *Chem. Rev.*, 2020, **119**, 12422–12490.
18 L. Lui, R. M. Ward and J. M. Schomaker, Regioselective intramolecular allene amidation enabled by an EDA complex, *Chem.–Eur. J.*, 2020, **26**, 13783–13787.
19 R. Y. Tien and P. I. Abell, Kinetics and stereochemistry of the gas-phase addition of HBr to methyl-substituted allenes, *J. Org. Chem.*, 1970, **35**, 956–960.
20 E. Heiba, The chemistry of allene. I. Factors governing the orientation of free-radical addition, *J. Org. Chem.*, 1966, **31**, 776–780.
21 K. Griesbaum, A. A. Oswald, E. Quiram, W. Naegele and C. I. Allene, Free Radical Addition of Thiols to Allene, *J. Org. Chem.*, 1963, **28**, 1952–1957.
22 J. E. Baldwin, Rules for ring closure, *J. Chem. Soc., Chem. Commun.*, 1976, 734–736.
23 J. J. A. Garwood, A. D. Chen and D. A. Nagib, Radical Polarity, *J. Am. Chem. Soc.*, 2024, **146**, 28034–28059.
24 G. L. Lackner, K. W. Quasdorf and L. E. Overman, Direct construction of quaternary carbons from tertiary alcohols *via* photoredox-catalyzed fragmentation of *tert*-alkyl *N*-phthalimidoyl oxalates, *J. Am. Chem. Soc.*, 2013, **135**, 15342–15345.
25 C. C. Nawrat, C. R. Jamison, Y. Slutskyy, D. W. C. MacMillan and L. E. Overman, Oxalates as activating groups for alcohols in visible light photoredox catalysis: formation of quaternary centers by redox-neutral fragment coupling, *J. Am. Chem. Soc.*, 2015, **137**, 11270–11273.
26 W. Li, Y. Jiang, Y. Li and J. Xia, Photoredox Ni-catalyzed selective coupling of organic halides and oxalates to esters *via* alkoxycarbonyl radical intermediates, *CCS Chem.*, 2022, **4**, 1326–1336.
27 M. Giustiniano, C. Russo and C. Volpe, The multiple facets of oxalate dianion in photochemistry, *ChemPhotoChem*, 2025, e202400407.
28 N. A. Weires, Y. Slutskyy and L. E. Overman, Facile preparation of spirolactones by an alkoxycarbonyl radical cyclization cross-coupling cascade, *Angew. Chem., Int. Ed.*, 2019, **58**, 8561–8565.
29 Q. Zhu, D. E. Graff and R. R. Knowles, Intermolecular anti-Markovnikov hydroamination of unactivated alkenes with sulfonamides enabled by proton-coupled-electron transfer, *J. Am. Chem. Soc.*, 2018, **140**, 741–747.
30 N. A. Romero and D. A. Nicewicz, Mechanistic insight into the photoredox catalysis of anti-Markovnikov alkene hydrofunctionalization reactions, *J. Am. Chem. Soc.*, 2014, **136**, 17024–17035.

31 W. M. Haynes, *CRC Handbook of Chemistry and Physics*, CRC Press, 2019.
32 B. G. Cox, *Acids and Bases Solvent Effects on Acid-Base Strength*, Oxford University Press, 2003.
33 E. P. Geunes, J. M. Meinhardt, E. J. Wu and R. R. Knowles, Photocatalytic anti-Markovnikov hydroamination of alkenes with primary heteroaryl amines, *J. Am. Chem. Soc.*, 2023, **145**, 21738–21744.
34 F. Dénès, M. Pichowicz, G. Povie and P. Renaud, Thiyl radicals in organic synthesis, *Chem. Rev.*, 2014, **114**, 2587–2693.
35 H. Togo, *Advanced Free Radical Reactions for Organic Synthesis*, Elsevier, 2021.
36 For Stern–Volmer experimental setup and procedures, see: W. B. Swords, H. Lee, Y. Park, F. Llamas, K. L. Skubi, J. Park, I. A. Guzei, M. Baik and T. P. Yoon, Highly Enantioselective 6π Photoelectrocyclizations Engineered by Hydrogen Bonding, *J. Am. Chem. Soc.*, 2023, **145**, 27045–27053.
37 I. V. Alabugin, P. Eckhardt, K. M. Christopher and T. Opatz, The photoredox paradox: electron and hole upconversion as the hidden secrets of photoredox catalysis, *J. Am. Chem. Soc.*, 2024, **146**, 27233–27254.
38 Y. Zhang, X. Gu and A. E. Wendlandt, A Change from Kinetic to Thermodynamic Control Enables *trans*-Selective Stereochemical Editing of Vicinal Diols, *J. Am. Chem. Soc.*, 2021, **144**, 599–605.
39 Y. Zhang, V. Palani, A. E. Seim, K. J. Wang and A. E. Wendlandt, Stereochemical editing logic powered by the epimerization of unactivated tertiary stereocenters, *Science*, 2022, **378**, 383–390.
40 K. Gach and A. Janecka, α-methylene-γ-lactones as a Novel Class of Anti-leukemic Agents, *Anti-Cancer Agents Med. Chem.*, 2014, **14**, 688–694.
41 T. G. Back, M. V. Krishna and K. R. Muraludharan, Preparation of allenic sulfones and allenes from the selenosulfonation of acetylenes, *J. Org. Chem.*, 1989, **54**, 4146–4153.
42 (First ESI† reference) E. P. Geunes, J. M. Meinhardt, E. J. Wu and R. R. Knowles, Photocatalytic anti-Markovnikov hydroamination of alkenes with primary heteroaryl amines, *J. Am. Chem. Soc.*, 2023, **145**, 21738–21744.
43 W. L. F. Armarego and C. L. L. Chai, *Purification of Laboratory Chemicals*, Elsevier, 6th edn, Burlington, MA, 2009.
44 W. C. Still, M. Kahn and A. J. Mitra, Rapid Chromatographic Technique for Preparative Separations with Moderate Resolution, *J. Org. Chem.*, 1978, **43**, 2923–2925.
45 A. M. Haydl and B. Breit, Atom-Economical Dimerization Strategy by the Rhodium-Catalyzed Addition of Carboxylic Acids to Allenes: Protecting-Group-Free Synthesis of Clavosolide A and Late-Stage Modification, *Angew. Chem., Int. Ed.*, 2015, **54**, 15530–15534.
46 C. Yao, A. D. N. Williams, Y. Gu and J. N. Norton, Isomerization of Aziridines to Allyl Amines *via* Titanium and Chromium Cooperative Catalysis, *J. Org. Chem.*, 2022, **87**, 4991–4997.
47 E. Benedetti, G. Lemière, L. Chapellet, A. Penoni, G. Palmisano, M. Malacria, J. Goddard and L. Fensterbank, Gold(I)-Catalyzed Cyclization of β-Allenylhydrazones: An Efficient Synthesis of Multisubstituted N-Aminopyrroles, *Org. Lett.*, 2010, **12**, 4396–4399.
48 P. A. Spreider and B. Breit, Palladium-Catalyzed Stereoselective Cyclization of *in Situ* Formed Allenyl Hemiacetals: Synthesis of Rosuvastatin and Pitavastatin, *Org. Lett.*, 2018, **20**, 3286–3290.
49 S. Grimme, J. Antony, S. Ehrlich and H. Krieg, A Consistent and Accurate *Ab Initio* Parametrization of Density Functional Dispersion Correction (DFT-D) for the 94 Elements H-Pu, *J. Chem. Phys.*, 2010, **132**, 154104.
50 **https://organicchemistrydata.org/hansreich/resources/nmr/?index=nmr_index%2Finfo&page=06-cmr-03-shift-effects%2F#06-cmr-03-shift-effects-gamma** from the Reich collection.